Monte-Carlo Evaluation of Uncertainties of UV Spectra Measured with Brewer Spectroradiometers

C. González[1,2], J. M. Vilaplana[1], and A. Serrano[2]

[1]Área de investigación e Instrumentación Atmosférica, Instituto Nacional de Técnica Aeroespacial (INTA), El Arenosillo, Huelva, Spain.

[2]Departamento de Física, Instituto del Agua, Cambio Climático y Sostenibilidad, Facultad de Ciencias, Universidad de Extremadura, Badajoz, Spain.

Corresponding author: Carmen González (cgonher@inta.es)

Key Points:

- A Monte Carlo technique has been implemented to obtain the uncertainty of the spectral ultraviolet recorded by a Brewer MKIII spectrometer.
- The methodology used for the uncertainty propagation is general and can be adapted to most spectroradiometers used in UV research.
- Brewer spectrometers are suitable for model and satellite validation but might be limited in the determination of spectral UV trends.

Abstract

Precise spectral ultraviolet (UV) measurements are needed to ensure human protection as well as to support scientific research. Quantifying the uncertainty of the UV spectra recorded is crucial to evaluate the quality of the measurements which is needed, in turn, for the assessment of their reliability. However, for double-monochromator spectroradiometers, the analytical derivation of this uncertainty is a challenging task due to the difficulties involved in propagating individual uncertainties. Under these circumstances, a Monte Carlo simulation is a reliable alternative as it does not require the calculation of partial derivatives and considers both nonlinear effects and correlations in the data. In the present study, the uncertainty of the spectral UV irradiance measured by a Brewer MKIII spectrophotometer is evaluated using a Monte-Carlo approach. This instrument belongs to the National Institute of Aerospace Technology and has successfully participated in several international campaigns, which ensures its precise calibration. The average expanded uncertainty (k = 2) of the global UV irradiance measured by this instrument varies between 10 % at 300 nm and 7 % at 363 nm. At shorter wavelengths, it increases sharply due to thermal and electronic noise as well as wavelength misalignment. The results indicate that a Brewer spectrophotometer is suitable for climatological studies and model validation. Nevertheless, a substantial reduction of these uncertainties might be required for accurately detecting long-term UV trends. Although the study focused on a Brewer spectrometer, the methodology used for the uncertainty analysis is general and can be adapted to most UV spectroradiometers.

Plain Language Summary

The solar ultraviolet (UV) spectrum covers the wavelength range from 100 to 400 nm. Although it represents less than 10 % of the total radiation reaching the earth's surface, it is of great importance as it can be harmful to humans, aquatic, and terrestrial ecosystems. To study its effects, high-quality measurements are needed. To determine the quality of the irradiance recorded its uncertainty must be first evaluated. Most techniques used for uncertainty estimation rely on the calculation of partial derivatives, which are difficult to obtain for most instruments measuring UV irradiance. The reason for this is that the mathematical expression relating some uncertainty sources and the measured irradiance is complex, with unknown correlations between the different uncertainty sources. To solve this problem, the Monte Carlo technique was used instead of the analytical one. The Monte Carlo approach is easier to implement and needs no calculation of partial derivatives. The method was implemented for a Brewer spectrometer, one of the preferred devices to measure UV irradiance. The results indicate that the Brewer is suitable for model validation, but a substantial reduction of its uncertainty might be needed to accurately detect spectral UV trends.

1 Introduction

The discovery of stratospheric ozone depletion over Antarctica and midlatitudes in the 1980s (Farman et al., 1985; Harris et al., 1997) stimulated the deployment of large ultraviolet radiation (UV) monitoring networks. Since ozone attenuates UV radiation, the widespread depletion resulted in a rise of surface UV levels, such as the increases reported by several stations during

the 1990s (Kerr & McElroy, 1993; McKenzie et al., 1999; Seckmeyer et al., 1994; Zerefos et al., 1997). The regulation on ozone-depleting substances agreed in the Montreal Protocol decelerated the decrease in ozone levels (Morgenstern et al., 2008; Newman et al., 2009; Prather et al., 1996). Nevertheless, surface UV irradiance could still increase if its other influential factors, such as clouds or aerosols, vary.

Potential changes in solar UV irradiance are of great environmental concern as this radiation may have detrimental effects on humans (Bais et al., 2018; D'Orazio et al., 2013; Hart & Norval, 2018; Lumi et al., 2021), materials (Andrady et al., 2023; Wachter el al., 2021) as well as terrestrial and aquatic ecosystems (Barnes et al., 2023; García-Corral et al., 2020; Neale et al., 2023). Since these harmful effects depend greatly on the wavelength, spectral UV measurements are needed to accurately appraise their risks. Furthermore, continuous monitoring is also vital to assess the possible variations in surface UV levels due to the forecasted changes in clouds, aerosols, and surface reflectivity. However, providing reliable estimations of such trends is a challenging task as it requires low-uncertainty spectral measurements (Arola et al., 2003; Bernhard, 2011; Glandorf et al., 2005; Weatherhead et al., 1998). In fact, Bernhard and Seckmeyer (1999) found that even if the lowest possible uncertainty was assumed, around 2 % for wavelengths below 320 nm, a double-monochromator spectroradiometer was unable to detect the change in erythemal UV due to a 1 % change in ozone. Therefore, high-quality measurements are needed, with uncertainties lower than 2 %.

To ensure low-uncertainty UV measurements, precise quality assurance (QA) and quality control (QC) procedures are essential. QA currently assesses the instrument's performance through intercomparison campaigns (e.g. Bais et al., 2001; Redondas et al., 2020). In particular, for solar UV measurements, the QASUME (Gröbner et al., 2005; Hülsen et al., 2016) acts as the traveling reference. Regarding QC, it is carried out at monitoring stations and includes identifying the uncertainty sources and evaluating the uncertainty of the measurements (Webb et al., 1998). Several studies have developed guides and recommendations to estimate UV irradiance uncertainty using the law of propagation of uncertainties (LPU) (Bernhard & Seckmeyer, 1999; Seckmeyer et al., 2001; Webb et al., 1998). Nonetheless, performing a complete evaluation of solar UV irradiance by applying LPU is highly complicated as it is difficult to provide the partial derivatives of the model used to derive the irradiance. Furthermore, it is unclear whether the uncertainty sources are correlated or if the model is linear. Under these circumstances, a Monte

Carlo simulation is a reliable alternative as it does not require the calculation of partial derivatives and takes into account both nonlinear effects (BIPM et al., 2008) and correlations (Kärhä et al., 2017) in the spectral data.

The Monte Carlo approach has been used to evaluate the uncertainty of spectral irradiance measurements obtained from both double monochromator-based (Cordero et al., 2008b; Vaskuri et al., 2018) and CCD-array-based spectroradiometers (Cordero et al., 2012; Schinke et al., 2020; Schmähling et al., 2018). As for the Brewer spectrophotometer, this methodology was applied to estimate the uncertainty of its nitrogen dioxide measurements (Diémoz et al., 2014). Nonetheless, the uncertainty of its spectral UV irradiance measurements is yet to be studied, even though these instruments have greatly contributed to the establishment of worldwide UV monitoring networks. In fact, Brewer spectrophotometers have been performing global UV irradiance measurements since the 1990s, enabling the investigation of long-term UV changes (De Bock et al., 2014; Fioletov et al., 2001; Fountoulakis et al., 2016a; Lakkala et al., 2017; Zerefos et al., 2012). Moreover, their measurements have also been used to study biologically effective UV dose rates (Fioletov et al., 2003; Kimlin, 2004), to assess the influence of atmospheric constituents on UV radiation (Bernhard et al., 2007; Seckmeyer et al., 2008), and to validate radiative transfer models (Mayer et al., 1997). Thus, this instrument has significantly served the scientific community for more than 30 years.

In this paper, an uncertainty analysis of the spectral UV irradiance measured by a Brewer MKIII spectrometer has been carried out using a Monte Carlo-based uncertainty propagation technique. The spectral measurements used were performed after the XVI Intercomparison campaign of the Regional Brewer Calibration Center – Europe (RBCC-E) at INTA / El Arenosillo.

The article is structured as follows. To begin with, Sect. 2 presents the technical characteristics of the double Brewer and its measuring procedure. Next, Sect. 3 describes the methodology as well as the characterization of the error sources considered in the analysis. Continuing with Sect. 4, where the Monte Carlo uncertainty evaluation is laid out. Finally, Sect. 5 summarizes the main conclusions.

2 Brewer MKIII spectrophotometer

The Brewer MKIII spectrophotometer with serial number 150 (hereafter "Brewer #150") is deployed at the "El Arenosillo" Atmospheric Sounding Station, belonging to the National Institute of Aerospace Technology (INTA). The Station is located in Mazagón, Huelva, Spain (37.1° N, 6.7° W, 41 m a.s.l.) and hosts, every 2 years, the RBCC-E calibration campaigns, where Brewers belonging to different institutions are calibrated for global UV irradiance and total ozone column (TOC).

The fully-automated Brewer #150 is a double monochromator spectroradiometer manufactured by Kipp and Zonen (https://www.kippzonen.com/, last access: 7 June 2023), with headquarters in Delft, the Netherlands. It was installed at "El Arenosillo" in 1997 for the measuring of total ozone in column, aerosol optical depth, and solar spectral UV irradiance. Thanks to the quality of Brewer #150 spectral measurements, its UV dataset has been used in many studies such as validation of satellite products (Antón et al., 2010; Cachorro et al., 2010), broadband calibration (Antón et al., 2011; Cancillo et al., 2005), and intercomparison campaigns (Cachorro et al., 2002).

For Brewer #150 spectral UV irradiance measurements, the wavelength range is 290–363 nm, with a step of 0.5 nm. It has a triangular slit function with a Full Width at Half Maximum (FWHM) of 0.55 nm. With these settings, the duration of a scan is approximately 4.5 min. The instrument is housed in a weather-proof box with no temperature stabilization.

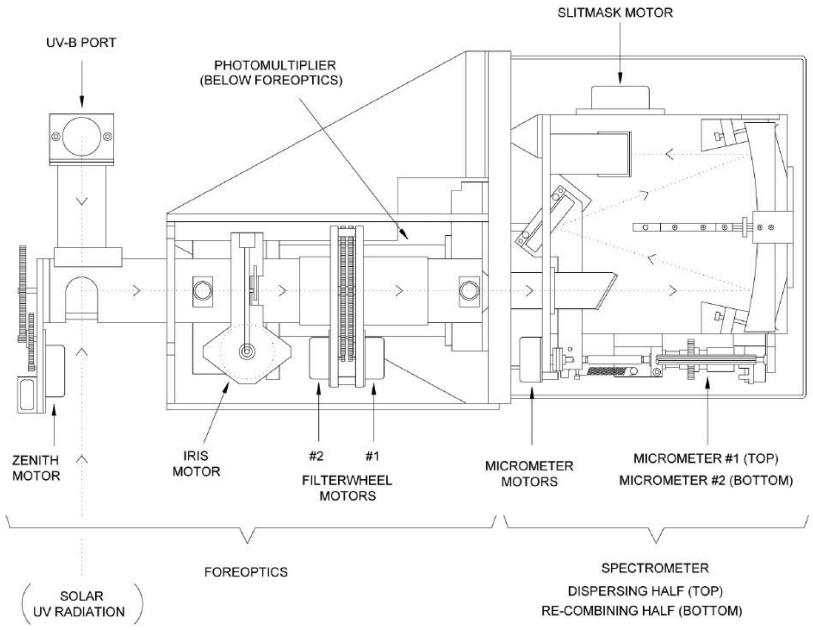

Figure 1: Top view of a Brewer MKIII spectrometer (Kipp and Zonen Brewer user manual)

To measure spectral UV irradiance, solar irradiance enters Brewer #150 through a CMS-Schreder entrance optic (model UV-J1015). It consists of a shaped Teflon diffuser covered by a quartz dome. This design is different from the standard entrance optic, a flat diffuser, and improves the Brewer angular response for global UV irradiance measurements (Gröbner, 2003). After passing through the diffuser, light is guided into the optical axis using a reflective prism. As seen in Fig. 1, the light subsequently enters the fore-optics, which comprises a set of quartz lenses and an iris diaphragm to focus and collimate the beam, as well as two filter wheels. The first filter wheel contains one open hole, for UV measurements, and an opaque disk, for dark count tests. The second wheel has five neutral density filters to ensure the Brewer signal is within appropriate levels. Thereafter, radiation is focused onto the spectrometer. Brewer #150 spectrometer is a modified Ebert type consisting of a pair of monochromators and a slit mask placed in front of the exit slit plane. For the measuring of ozone, dead time, and dark counts, the slit mask rotates to select the wavelength, while the diffraction gratings remain fixed. On the other hand, for UV observations, the slits are fixed, and the wavelength is selected by rotating the gratings, using two micrometers. The incoming light is dispersed in the first monochromator and then recombined in the second one, reducing in this way the stray light of the system. Finally, the photons are collected on the cathode of a low-noise photomultiplier tube (PMT). The

154 photon pulses are converted to counts per cycle. For Brewer measurements, the sampling time is
155 performed in cycles, with the slit mask rotating in front of the exit slit plane of the spectrometer.
156 In each position of the slotted mask, photons are allowed to reach the PMT during 0.1147 s
157 which is called the integration time.

158 The output signal of the above measuring procedure is affected by several error sources and must
159 be corrected before irradiance values can be derived. To convert the Brewer photon counts into
160 irradiances, the responsivities of the instrument must be known. For Brewer #150, its spectral
161 response is determined every year using several quartz-halogen tungsten 1000 W lamps with
162 certified spectral irradiance. To prevent any changes in the instrument during transportation, the
163 calibration is carried out using a mobile lamp system, placed on top of the instrument. The unit
164 has three flat baffles, between the reference lamp and the entrance optics, to eliminate stray light.
165 Furthermore, the whole system is covered by a black cloth to block external light. During the
166 radiometric calibration, the current of the lamp is controlled and recorded to monitor its stability.

167 The model used to derive the irradiance measured by Brewer #150 will be explained in Sect. 2.1.
168 and 2.2. It is formed by a set of equations that relate the uncertainty sources (dead time, dark
169 counts, temperature, etc.) to the final corrected irradiance. In the following, bold font will be
170 used to represent spectral variables (vectors).

171 **2.1 Radiometric calibration**

172 As mentioned earlier, the spectral responsivity $\boldsymbol{R}$ of the Brewer is determined by irradiating the
173 entrance optics with a reference lamp. To carry out the calibration, the distance between the lamp
174 and the reference plane of the diffuser needs to be the one stated in the lamp's calibration
175 certificate d_r. For the traditional design (a flat diffuser), this reference plane coincides with the
176 metallic ring that surrounds the quartz dome (see Fig. 2). However, Brewer #150 diffuser is
177 placed below this reference. As a result, the distance d between the lamp and the diffuser must be
178 adjusted to take into account this offset Δd (see Sect. 3.2.5)

179 $$d = d_r - \Delta d \ . \qquad (1)$$

180 Once the distance is correctly adjusted and the lamp is stabilized, the photon counts $\boldsymbol{L}_0$ are
181 recorded in counts cycle^{-1}. The raw counts detected by the PMT are a sum of counts generated
182 from UV photons as well as those arising from thermal noise, usually referred to as "dark

counts" (see Sect. 3.2.3). Therefore, the raw counts $\boldsymbol{L}_0$ must be corrected by subtracting the dark counts D_L. Regarding stray light, no correction is needed for a double Brewer (Bais et al., 1996), assuming that most of the stray light is rejected by the second spectrometer.

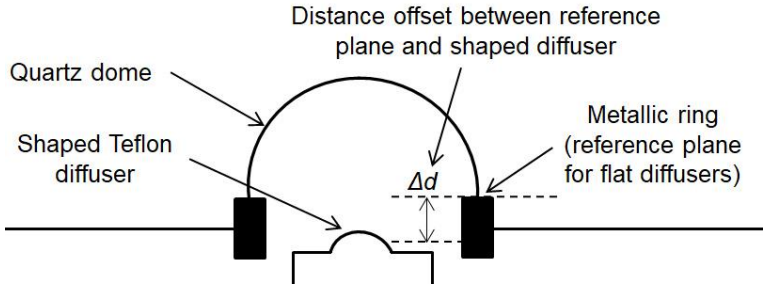

Figure 2: Schematic drawing of transversal cut of Brewer #150 curved diffuser.

Following the algorithm set in Brewer's manual, the raw counts must be converted to count rates $\boldsymbol{L}_1$ (counts s^{-1}). At each wavelength i¸ where i = 290–363 nm, the count rate is calculated as

$$L_{1,i} = \frac{2(L_{0,i} - D_L)}{C \cdot t}, \quad (2)$$

where t is the integration time and C the number of cycles of the measurement. The integration time is 0.1147 s for all types of measurements while the number of cycles depends on the type of observation and wavelength. For lamp measurements, the number of cycles is 30 for wavelengths below 300 nm and 20 for wavelengths above 300 nm.

Next, the counts need to be corrected for non-linearity. For Brewer spectrometers, the main cause of nonlinearity is the dead time τ (see Sect. 3.2.4), a time period where the photomultiplier is unable to detect any incoming photons. Assuming Poisson statistics, the corrected signal values $\boldsymbol{L}_2$ are obtained in an iterative process (n = 0…9)

$$L_{2,i}(\mathrm{n}+1) = L_{1,i} \cdot e^{L_{2,i}(n) \cdot \tau}, \quad (3)$$

where $L_{2,i}(0) = L_{1,i}$.

Finally, the spectral responsivity of the instrument $\boldsymbol{R}$ can be obtained as

$$R_i = L_{2,i} / E_{L,i}, \quad (4)$$

where $E_{L,i}$ is the spectral irradiance emitted by the reference lamp

2.2 Spectral irradiance

To obtain solar irradiance measurements, Brewer #150 is placed outdoors and the raw counts under the Sun are measured $\boldsymbol{S}_0$. This signal might be affected by spikes, an unusual number of counts recorded that do not arise from the incident radiation. To detect and correct them, the methodology set by Meinander et al. (2003) has been applied. Furthermore, the outdoors signal values must also be corrected, similarly to the ones obtained during the calibration, for dark counts D, converted to count rate $\boldsymbol{S}_1$ (in counts s^{-1}), and corrected for dead time $\boldsymbol{S}_2$ (in counts s^{-1})

$$S_{1,i} = \frac{2(S_{0,i}-D)}{C \cdot t}\,, \tag{5}$$

$$S_{2,i}(\mathrm{n}+1) = S_{1,i} \cdot e^{S_{2,i}(n)\cdot\tau}\,. \tag{6}$$

For UV observation, the number of cycles is different, 4 cycles for wavelengths below 300 nm and 2 cycles for wavelengths above 300 nm. Once the count rates are obtained, they are converted into spectral irradiance $\boldsymbol{E}_0$ using the responsivity values of the instrument $\boldsymbol{R}$, determined during the absolute calibration (as described in the previous section)

$$E_{0,i} = S_{2,i}/R_i\,. \tag{7}$$

Nevertheless, the spectral irradiance measured by a Brewer spectrometer needs further processing. As mentioned earlier, Brewer #150 has no temperature stabilization system. Consequently, its UV measurements have a linear dependence for temperature (see Sect. 3.2.9) and the irradiance values must be corrected $\boldsymbol{E}_1$ using

$$E_{1,i} = E_{0,i}/(1 + c_\mathrm{t} \cdot \Delta T)\,, \tag{8}$$

where c_t is the temperature correction factor and ΔT is the difference between the reference temperature and the temperature of the scan.

Furthermore, the irradiances must also be corrected for its non-ideal angular response $\boldsymbol{E}_2$. Brewer #150 angular response was measured in the laboratory to obtain its cosine error at each wavelength. Once this error is determined, the spectral cosine correction function ***A(SZA)*** can be simulated (see Sect. 3.2.10) and the irradiances are corrected by simply multiplying

$$E_{2,i} = E_{1,i} \cdot A_i\,. \tag{9}$$

3 Irradiance uncertainty analysis

3.1 Methodology

For the uncertainty evaluation, the measurements performed by Brewer #150 from 10 September to 20 October 2021 have been used. These measurements were obtained after a calibration took place, specifically during the XVI Intercomparison campaign of the RBCC-E (from 6 September to 15 September 2021) held at "El Arenosillo" Observatory. The study period was extended, until 20 October, to include the maximum number of cloud-free conditions possible. Cloudy conditions have not been considered since they strongly affect surface UV radiation (Schafer et al., 1996) and scanning spectrometers, such as Brewer #150, do not have enough temporal resolution to properly detect these fast changes. On the other hand, the study period could not be extended any further since, for later dates, the temperature of Brewer #150 was, for most UV scans, lower than 23 °C, which is the limit of the temperature interval where its correction is characterised. Therefore, UV measurements recorded after 20 October 2021 have not been considered as their temperature dependence cannot be corrected. Putting the former criteria into practice resulted in 599 cloud-free UV spectra.

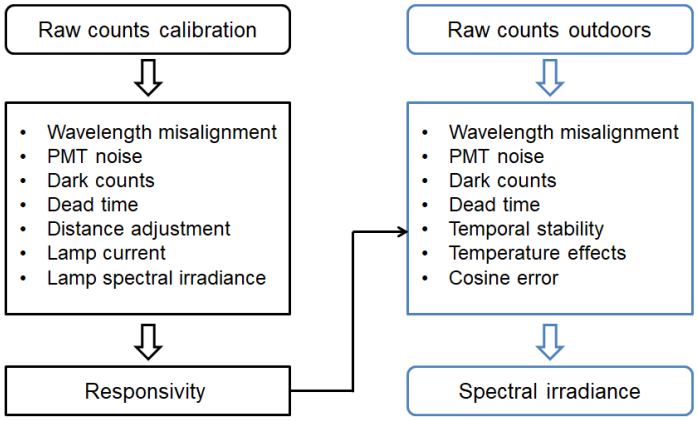

Figure 3: Schematic representation of the uncertainty sources affecting the spectral irradiance measured by Brewer #150. The left branch describes the uncertainties that affect the radiometric calibration and the right branch the ones involved in the field measurements.

To determine the combined standard uncertainty of the spectral UV irradiance measured by Brewer #150, the methodology set in the Supplement 1 to the Guide to the Expression of Uncertainty in Measurement (GUM) has been followed (BIPM et al., 2008). This consists of a Monte Carlo simulation that obtains the total uncertainty in three steps by identifying (1) the

uncertainty sources affecting the measurements, (2) their probability density functions (PDFs), and (3) the measurement model that relates the spectral irradiance with the uncertainty sources (described in detail in Sect. 2.1 and 2.2). The uncertainty sources for Brewer #150 are shown in Fig. 3. Their PDFs and how they affect the measurements will be discussed in the following Sect. 3.2. Once the three steps are completed, the spectral irradiance is calculated many times while varying the uncertainty sources according to their PDFs. For this study, the number of iterations was $N = 10^5$. The Monte Carlo simulation was implemented using two nested loops: one for the 10^5 Monte-Carlo iterations and another one that goes through all the wavelengths (290–363 nm). If the uncertainty source depends on the wavelength (such as cosine error, PMT noise or temporal stability), its values are drawn on the inner loop. In this way, the spectral sources are varied independently at each wavelength. On the other hand, if the uncertainty sources have no spectral dependency, such as dead time, dark counts, or temperature correction, they are varied on the outer loop. The simulation then renders a set of values of spectral irradiance $\boldsymbol{E}_{\mathrm{S},1}...\boldsymbol{E}_{\mathrm{S,N}}$ that allows the calculation of the estimate $\boldsymbol{E}_{\mathrm{M}}$ and their associated uncertainties $\boldsymbol{u}_{\mathrm{M}}$

$$\boldsymbol{E}_{\mathrm{M}} = \frac{1}{N}\sum_{j=1}^{N} \boldsymbol{E}_{\mathrm{S},j} \,, \tag{10}$$

$$\boldsymbol{u}_{\mathrm{M}} = \left(\frac{1}{(N-1)}\sum_{j=1}^{N}\left(\boldsymbol{E}_{\mathrm{S},j} - \boldsymbol{E}_{\mathrm{M}}\right)^2\right)^{1/2} . \tag{11}$$

Moreover, the PDF of the spectral irradiance can also be obtained by calculating the histogram of $\boldsymbol{E}_{\mathrm{S},j}$. If it is a normal distribution, the expanded uncertainties $\boldsymbol{U}_{\mathrm{M}}$ can be obtained by multiplying the combined standard uncertainties with a coverage factor of $k = 2$.

3.2 Uncertainty sources

This section describes the characterization and determination of the uncertainty sources used for the uncertainty analysis. Two main probability density functions (PDF) have been considered: the rectangular and the Gaussian. The rectangular PDF is used for those variables that range within a certain interval of values without any preferred value. This is the case, for example, of wavelength misalignment due to the position of the micrometer. The step of this micrometer corresponds to 0.004 nm and, therefore, any wavelength within the micrometer position plus or minus 0.004 nm is equally possible. In this case, the rectangular PDF is the most suitable. On the

other hand, there are variables with a clearly more probable value and an associated uncertainty that decreases as one departs from this more probable value. For these variables, a Gaussian PDF is more appropriate. An example of such a PDF is the number of dark counts. This number is estimated by measuring several times with the Brewer covered by a black cloth. The histogram of the resulting values shows a unimodal probability distribution that is adequately described by a Gaussian PDF. The mean and standard deviation are reliable estimates of the most likely value and the uncertainty of the distribution, respectively. The associated PDFs and their values are listed in Table 1.

Table 1: Summary of the probability density functions (PDFs) assigned to the different uncertainty sources affecting the Brewer UV irradiance measurement.

Uncertainty source	PDF
Wavelength misalignment (nm)	Described by two contributions: (1) Rectangular over the interval (–0.004, 0.004) (2) Rectangular over the interval defined by the spectral shift
Signal noise (counts $cycle^{-1}$)	Gaussian centred at the number of raw counts measured with standard deviations defined by the signal-to-noise-ratio
Dark counts (counts $cycle^{-1}$)	Gaussian centred at dark counts measured with a constant standard deviation relative to the counts (40 %)
Dead time (ns)	Gaussian centred at 26.7 with standard deviation 1.6
Distance adjustment (cm)	The uncertainty in the distance (50 cm) is described by two contributions: (1) Gaussian centred at 0 with standard deviation 0.015 (2) Rectangular over the interval (–0.1, 0.1)
Lamp current (A)	Rectangular over the interval (7.999, 8.001)

Lamp spectral irradiance (W m^{-2} nm^{-1})	Gaussian centred at $\boldsymbol{E}_L$ with the standard deviations indicated in the calibration certificate
Temporal stability (counts m^2 nm s^{-1} W^{-1})	Gaussian centred at $\boldsymbol{R}$ with the standard deviations obtained from consecutive calibrations $\boldsymbol{u}_R$
Temperature coefficient (% $°C^{-1}$)	Gaussian centred at –0.156 with standard deviation 0.023
Cosine correction	Uniform distribution over the cosine corrections obtained with variable values of SZA, ozone and aerosols

3.2.1 Wavelength misalignment

Due to ozone absorption the solar UV spectrum decreases sharply in the UVB region. As a result, small errors in the assigned wavelength of a spectrometer produce large deviations in its measured irradiance. To correct these wavelength misalignments a wavelength calibration must be performed before field measurements. This can be carried out by two methods: (1) comparing the wavelengths measured by the spectroradiometer against those corresponding to emission lines of several discharge lamps, such as mercury (Hg), cadmium (Cd), or zinc (Zn); (2) matching the Fraunhofer lines of the measured spectra with the respective ones in high-resolution reference spectra.

For Brewer #150, the wavelength calibration is carried out every two years following the procedures used by the RBCC-E (Gröbner et al., 1998; Kerr, 2002) at the calibration campaigns. In these procedures, the relation between the grating position and the actual wavelength of the monochromator is established by scanning spectral discharge lamps, usually Hg, Cd, and Zn. Furthermore, the resulting calibration is also checked using the Fraunhofer structure to determine wavelength shifts.

The standard uncertainty of this wavelength setting has two components: (1) the precision of the micrometer step setting and (2) the wavelength shifts. For Brewer spectrophotometers, the first contribution is approximately 8 pm (Gröbner et al., 1998). Therefore, according to the principle of maximum entropy (PME) (BIPM et al., 2008), the first component can be described by a rectangular distribution over the interval (–0.004, 0.004) nm. As for the wavelength shifts, they can be derived from the wavelength calibration, either with discharge lamps or by comparison

against the Fraunhofer structure. Similar wavelength shifts were found using the two methods, of the order of 0.01 nm at 300 nm. However, by matching the Fraunhofer lines, a specific spectral shift for each scan can be obtained. Therefore, shifts derived in this way were considered more accurate. Consequently, on each iteration, the wavelength scale was modified by

$$\lambda'_i = \lambda_i + u_{\mathrm{w}} + z_i \,, \tag{12}$$

where λ_i are the wavelengths measured by Brewer #150 (290–363 nm), u_{w} is described by a rectangular PDF over the interval (-0.004, 0.004) nm, and z_i is a rectangular distribution over the interval limited by the spectral shift for each wavelength. Spectral shifts were derived using the SHICRivm software package V. 3.075 (Slaper et al., 1995).

3.2.2 PMT noise

Due to noise in the spectroradiometer signal, repeated measurements of the same irradiance level will lead to slightly different results. For Brewer spectrophotometers, this noise mainly arises from the quantized nature of the electrons produced in the PMT's cathode. Therefore, the raw counts measured by Brewer #150, both during the calibration $\boldsymbol{L}_0$ and outdoors $\boldsymbol{S}_0$, are affected by this noise.

To characterise Brewer #150 noise during the calibration, the recommendations stated in Bernhard and Seckmeyer (1999) were followed, i.e. the signal-to-noise-ratio S/N was derived from consecutive measurements of a 1000 W lamp. For solar measurements, S/N is hard to accurately determine, as it depends on wavelength, SZA, and atmospheric variability. Nevertheless, an upper limit was estimated from a group of near measurements at each wavelength. The S/N measured, both during the calibration and measurements outdoors, decreases rapidly as wavelength increases. For the 310–360 nm wavelength region, it levels off at 3 % and 0.11 % for the 1000 W lamp and field measurements, respectively.

To simulate the PMT noise, the raw counts measured by the Brewer were modified on each iteration by sampling from a normal distribution centred at the raw counts recorded with standard deviations defined by the signal-to-noise-ratio.

3.2.3 Dark counts

Dark counts are measured automatically by setting the rotating slit mask at position 1, blocking all the slits and, in turn, blocking all incoming light. They are recorded before each UV scan. Since Brewer #150 is not stabilized in temperature, dark counts fluctuate throughout the day.

To characterise the dark counts measured by Brewer #150, the instrument was covered with a black cloth and performed ten UV scans at 30 °C. The results showed no spectral dependency. To estimate an uncertainty for the obtained dark counts of 0.5 counts per cycle, a standard deviation for the ten scans performed was calculated. This standard deviation, 0.2 counts per cycle, represented 40 % of the dark counts measured. Therefore, on each Monte Carlo iteration, the dark current was described by a normal PDF centred at the dark counts measured with a constant standard deviation relative to the counts (40 %), in an attempt to simulate the effect temperature has on dark counts Although the uncertainty evaluation is more precise in this way, introducing the temperature effects has no considerable impact on the total uncertainty budget. After varying the dark counts, the Brewer signal was corrected as indicated in Eq. (2) and (5).

3.2.4 Dead time

The cause of nonlinearity in Brewer spectrophotometers is the loss of photons due to the dead time τ of the photomultiplier. This constant is a measure of how long the detection system is 'dead', i.e. it is the time after detecting a photon during which the PMT is unable to detect a second one. It is specific for each instrument as its value depends on the configuration and type of PMT used.

Brewer spectrophotometers can measure their dead time automatically by comparing the count rates when two slits are opened simultaneously to the counts registered when the slits are opened individually. A complete description of the algorithm used to derive the dead time and its calculation can be found in Fountoulakis et al. (2016b).

Brewer #150 measures its dead time every day by performing a DT test. This test determines the dead time several times for high and low intensities of the internal standard lamp. Then, the mean and standard deviation are recorded in a file for both high- and low-intensity cases. According to the Brewer's manual both measurements should agree within two standard deviations and lie in the range 20–35 ns. For the period of study, the mean dead time was 26.7 ns and its standard uncertainty 1.6 ns. If only high-intensity cases are considered, then the standard

uncertainty of the dead time is 0.9 ns, in agreement with the findings of Fountoulakis et al. (2016b).

In the Monte Carlo simulation, the DT is modified on each iteration by sampling from a Gaussian distribution centred at 26.7 ns with standard deviation of 1.6 ns. Once the DT is determined, the Brewer count rates, $\boldsymbol{L}_1$ and $\boldsymbol{S}_1$, were corrected for nonlinearity using Eq. (3) and (6).

3.2.5 Distance adjustment

During the calibration, the response values of the spectroradiometer are obtained using the spectral irradiance of the lamp, as indicated in Eq. (4). However, to ensure the lamp is emitting those irradiance values the distance between the reference lamp and the optical plane of the diffuser must be the one stated in the calibration certificate. Consequently, errors committed in this distance adjustment will lead to systematic errors in the measurements (Gröbner & Blumthaler, 2007; Hovila et al., 2005; Manninen et al., 2006;).

As shown in Fig. 2., Brewer #150 diffuser is placed below the used reference for calibration. To estimate the actual height of the diffuser, the spectrum emitted by an ultrastabilized lamp was measured at several distances. The results showed that the reference plane of the diffuser is situated $\Delta d = (0.234 \pm 0.015)$ cm below the metallic ring of the quartz dome. Therefore, Brewer #150 calibration needs to be performed by placing the reference lamp 0.23 cm below the distance specified in its calibration certificate. For 1000 W lamps this distance is 49.766 cm.

In the Monte Carlo simulation, the standard uncertainty committed in the distance adjustment has two components: (1) the precision of the instrument used (e.g. a ruler, a micrometer gauge) for measuring the distance and (2) the standard uncertainty of the offset Δd previously measured. For Brewer #150, the first contribution is described by a rectangular distribution over the interval (–0.1, 0.1) cm. It is to note that this source of uncertainty could be easily improved by acquiring a more precise ruler or micrometer gauge. The second one can be described by a gaussian distribution centred at 0 cm with standard deviation 0.015 cm, as obtained experimentally. It should be noticed that since the distance offset is modified, the distance between the lamp and the diffuser is no longer the one stated in the calibration certificate. Accordingly, the spectral irradiance changes and must be corrected using the inverse square law

$$E'_{\mathrm{L},i} = E_{\mathrm{L},i}\left(\frac{d_\mathrm{r}}{d_\mathrm{r} + u_\mathrm{d}}\right)^2, \quad (13)$$

where $E'_{\mathrm{L},i}$ are the calculated irradiances of the reference lamp, d_r is the reference distance (for 1000 W lamps is 50 cm) and u_d is the combined standard uncertainty of the offset obtained by adding the two components previously described.

Equation (13) is only valid if the distance between the lamp and the diffuser is sufficiently large. In the Monte Carlo simulation, the distance varies between 49.8 and 50.2 cm. Therefore, the lamp can still be regarded as a point source and Eq. (13) holds.

3.2.6 Lamp current

During the radiometric calibration, the reference lamp must be operated at the current specified in its calibration certificate. Maintaining constant the lamp current is essential since any deviations will lead to different spectral irradiance values than those stated in the lamp's calibration certificate (Webb et al., 1994).

According to Schinke et al. (2020) the variation in spectral irradiance due to changes in the operating current can be estimated by modelling the lamp as a black body radiator whose temperature is obtained from the following linear approximation

$$R(T) = R_0\big(1 + \alpha(T - T_0)\big), \quad (14)$$

where $R(T)$ is the resistance of the lamp's filament at the operating temperature, R_0 is the resistance at room temperature T_0, and α denotes the temperature coefficient of the filament. The resistance at operating temperature can be easily derived since the lamp voltage and current are monitored throughout the whole calibration process. For Brewer #150 setup, the mean resistance is $R(T)$ = 14.26 Ω. On the other hand, the resistance and room temperature were measured before the calibration took place, obtaining a room temperature of T_0 = 300.5 K and a corresponding resistance of R_0 = 0.89 Ω. Regarding the temperature coefficient α, it was derived in the laboratory by varying the lamp current at six different fixed values, from 6 to 8 A, and measuring, at each current level, the spectral irradiance emitted by the lamp ten times. For each current value, the temperature of the lamp was estimated using Planck's law and the resistance was determined thanks to the monitored current and voltage values. The data showed that the lamp resistance depends linearly on the temperature with a slope of α = (0.00544 ± 0.00014) K^{-1}.

Introducing the previous values in Eq. (14) the 1000 W lamp was modeled as a black body with temperature 3089 K.

In the Monte Carlo simulation, the current was slightly modified on each iteration, varying in turn the spectral irradiance of the lamp (as described in Schinke et al. (2020)). The setup used for Brewer #150 calibration maintains the current constant at 8 A with an error of 1 mA. Therefore, according to the PME, the lamp current can be described by a rectangular PDF over the interval (7.999, 8.001) A.

3.2.7 Lamp spectral irradiance

The uncertainties of the spectral irradiance values emitted by the calibrating lamp $\boldsymbol{E}_{\mathrm{L}}$ must be considered in the uncertainty analysis. For the 1000 W lamp used in this study, the uncertainty values $\boldsymbol{u}_{\mathrm{L}}$ are specified in the calibration certificate and range from 1.74 % at 250 nm to 0.91 % at 450 nm. Since they correspond to a coverage factor of $k = 2$, the spectral irradiance of the reference lamp was described by a normal PDF centered at $\boldsymbol{E}_{\mathrm{L}}$ with standard deviations $\boldsymbol{u}_{\mathrm{L}}/2$.

3.2.8 Temporal stability

The responsivity of a spectroradiometer changes with time due to the aging of the instrument, mechanical instabilities arising from its transportation or storage, among other factors. Consequently, consecutive calibrations result in different values of responsivity. To characterise the drifts of Brewer #150, the calibration records from 2005 to 2021 have been analysed. No data from prior years have been considered since in 2005 the traditional entrance optic was replaced for the CMS-Schreder design, greatly affecting the response of the instrument.

As suggested in Bernhard and Seckmeyer (1999), the difference between consecutive calibrations has been obtained for every wavelength. The data was consistent with a normal distribution. Therefore, for each wavelength, a standard deviation $u_{\mathrm{R},i}$ was derived. For Brewer #150 these uncertainties range from 3.75 % at 290 nm to 3.24 % at 363 nm. On each iteration, the responsivity of Brewer #150 was altered by sampling a Gaussian distribution centred at $\boldsymbol{R}$ with standard deviations $\boldsymbol{u}_{\mathrm{R}}$.

3.2.9 Temperature

Brewer spectrophotometers have no temperature stabilization system and therefore, their responsivity, and in turn their global UV measurements, depend on temperature (Cappellani & Kochler, 2000; Garane et al., 2006; Lakkala et al., 2008). For Brewer MKIII spectrometers, this sensitivity could be due to the effects temperature has on the PMT response as well as on the Teflon diffuser transmittance (Ylianttila & Schreder, 2005).

The temperature dependence is characteristic of each instrument (Fountoulakis et al., 2017; Weatherhead et al., 2001) and needs to be corrected. However, there is no standard methodology to characterise or correct the Brewer UV measurements. Existing studies have tried to characterise this dependence by using different external lamps (50, 200, and 1000 W) and performing the measurements either outdoors (e.g. Cappellani & Kochler, 2000; Weatherhead et al., 2001) or inside a laboratory (e.g. Garane et al., 2006; Lakkala et al., 2008). Using the internal standard lamp of the Brewer may also lead to an unreliable characterization since the temperature dependence of this lamp is unknown (Weatherhead et al., 2001). Furthermore, in a recent study, Fountoulakis et al. (2017) found that 50 W lamps are also unsuitable for a thorough characterization as they are placed near the diffuser, affecting its temperature and eventually its performance. On the other hand, 200 and 1000 W lamps provided reliable results since their distance from the diffuser was long enough to prevent its warming.

Brewer #150 was characterised using a 100 W lamp, placed at 10 cm from the diffuser. To guarantee that the diffuser was not being heated by this external lamp, the test was repeated with a 1000 W lamp, placed at 50 cm of the diffuser. The measurements were performed outdoors while the internal temperature of the Brewer increased gradually as the Sun heated the instrument. During the scans, the current of the lamps remained stabilized to their operating current (8 A for the 1000 W lamp and 6.6 A for the 100 W lamp). Furthermore, before each scan, the 297 nm line of the internal Hg lamp was scanned to ensure wavelength stability. This characterization test was repeated on three different days, two with the 100 W lamp and the remaining day with the 1000 W lamp.

Using the temperature of the PMT, which is recorded by the Brewer during each scan, the change of the Brewer #150 responsivity with respect to temperature has been calculated. The data showed that the response of Brewer #150 decreases linearly with temperature and that the

results were consistent for the three different experiments performed. Indicative results for 325 nm are presented in Fig. 4. The temperature range measured was 23–38 °C.

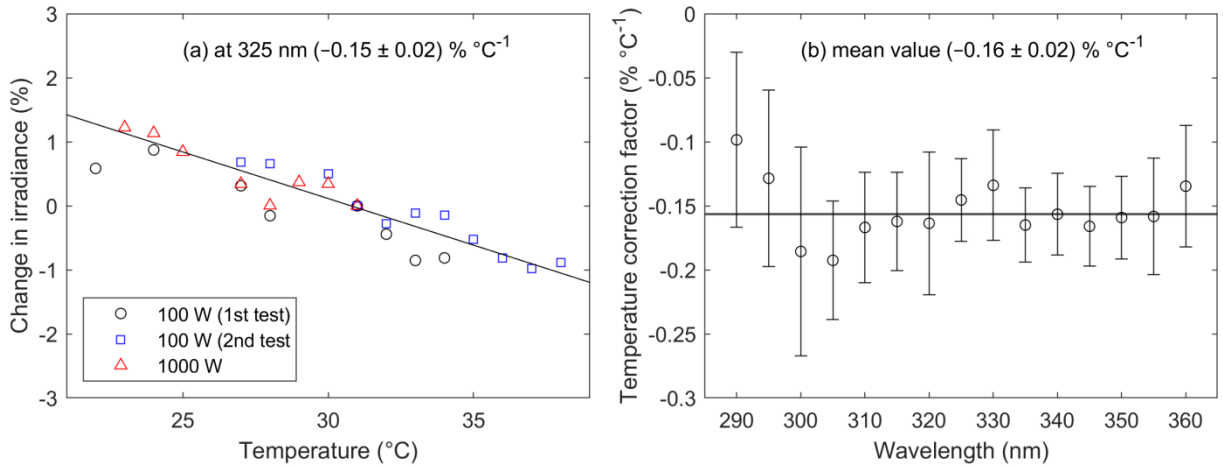

Figure 4: Results of the characterization in temperature for Brewer #150. (a) Change in irradiance (in %) at 325 nm with respect to the irradiance at 31 °C as a function of the Brewer's internal temperature. Measurements were performed outdoors using 100 and 1000 W lamps on three different days. (b) Wavelength dependence of the temperature correction, derived from linear fits.

It can be seen from Figure 4 that the temperature correction factor for Brewer #150 shows no spectral dependency. Thus, the average value, (–0.156 ± 0.023) % °C^{-1}, was chosen as the temperature correction factor for all the wavelength range. This value is similar to those obtained in previous studies (Fountoulakis et al., 2017; Garane et al., 2006; Weatherhead et al., 2001). Regarding the wavelength dependency, Garane et al. (2006) also obtained a correction factor with no spectral dependency. However, other studies have found a polynomial dependency for double monochromator Brewers (Fountoulakis et al., 2017; Lakkala et al., 2008). As already mentioned, the temperature dependence is characteristic of each Brewer and could be responsible for these differences.

Finally, in the Monte Carlo simulation, the temperature correction factor c_t is altered on each iteration by sampling from a normal distribution centred at –0.156 % °C^{-1} with standard deviation 0.023 % °C^{-1}. Irradiance values are then corrected by applying Eq. (8).

3.2.10 Cosine error

The cosine error is the deviation from the ideal angular response. Ideally, the irradiance measurements of a spectroradiometer should be proportional to the cosine of the angle between the direction of the incoming radiation and the normal of the diffuser. Brewer #150 angular response was measured in the laboratory in October 2019 and is represented in Fig. 5. To characterise the cosine error, the BAT (Brewer Angular Tester) device and a 150 W Xe arc lamp with an optic fibre were used.

The characterization was performed by placing the BAT device on top of the Brewer #150 diffuser. Once the lamp was stabilized, the angular response was measured at 315 nm for different zenith angles (starting from –85° to +85° by steps of 5°). Both orthogonal planes, North-South (NS) and West-East (WE), were measured twice. Using the angular response, the cosine error and its correction could be determined. The methodology followed was similar to the one described in Bais et al. (1998).

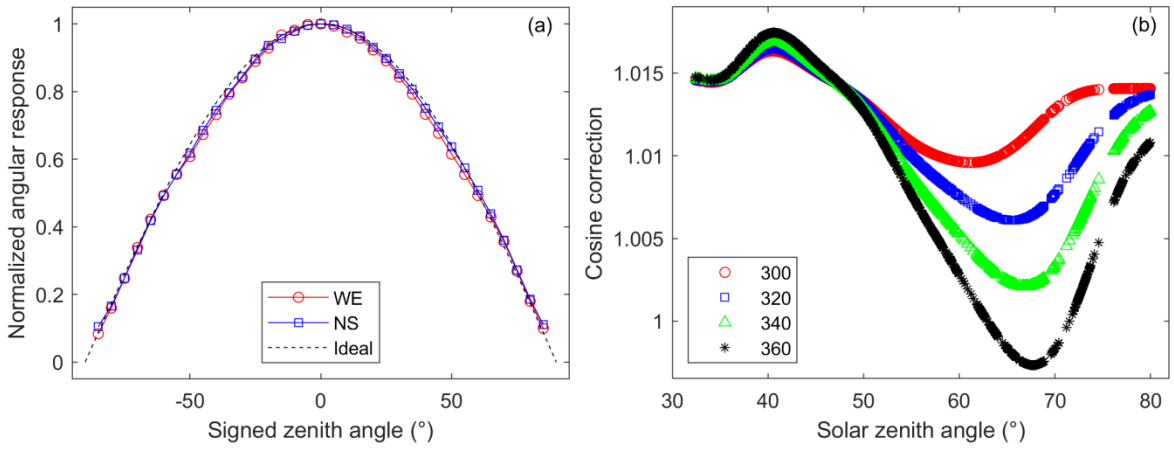

Figure 5: Cosine error characterization of Brewer #150. (a) Angular response measured for NS and WE planes and ideal response for different zenith angles at 315 nm. (b) Cosine correction for four wavelengths (300, 320, 340 and 360 nm) obtained for cloud-free skies and the mean values for columnar ozone and aerosols registered during the period of study.

Calculating this correction accurately is a hard task since it requires modelling the direct-to-global ratio, for each scan measured, using simultaneous ancillary measurements of aerosol content, ozone, and surface albedo. Therefore, it is usual to perform the simulation with typical or mean values of these atmospheric parameters (e.g. Fountoulakis et al., 2020; Cordero et al., 2008a). In this study, the influence of these assumptions will be analysed. Consequently, in Eq.

(9) the cosine correction used is the one obtained with the mean values of ozone (287.5 DU) and aerosols (1.371 and 0.039 alpha and beta Ångström exponents, respectively) of the study period and is shown in Fig. 5. On the other hand, the cosine correction was also calculated by modelling with simultaneous values of ozone and aerosols corresponding to each Brewer scan (variable parameters).

In the Monte Carlo simulation, the uncertainty of the cosine error will have two components: (1) the angular variability. A maximum error of 1° was estimated and (2) the error committed when ignoring the influence of aerosols and ozone in the model. Therefore, on each iteration, the cosine correction was obtained by sorting through the corrections calculated with atmospheric variable parameters and for the SZA of the corresponding scan ±1°.

4 Monte-Carlo simulated uncertainty

To analyse the combined standard uncertainty of Brewer #150 UV measurements, the standard deviations $\boldsymbol{u}_{\mathrm{M}}$ were evaluated considering the irradiance model, uncertainty sources, and values reported in Sect. 3. The data used correspond to 599 UV spectra measured under cloud-free conditions. The average Brewer #150 irradiance combined standard uncertainties for the wavelength range 290–363 nm as estimated by means of the Monte Carlo methodology are shown in Fig. 6.

The combined standard uncertainty shows a marked spectral dependency, growing considerably with wavelength. Thus, its mean value ranges from 0.005 mW m^{-2} nm^{-1} at 290 nm to 7.5 mW m^{-2} nm^{-1} at 320 nm. This increase in the absolute value of the combined standard uncertainty was expected since it follows the shape of the global UV irradiance arriving at Earth's surface. The variability of the uncertainty can be described by the range between the 5th and 95th percentiles (Fig. 6a). It rises gradually with wavelength until 320 nm, where it almost levels off. Its relative value exceeds 110 % below 320 nm and around 90 % hereafter.

The dependence of the combined standard uncertainty on solar angle was investigated by comparing its values for three different angles for the same date, 10 September 2021 (Fig. 6b). The uncertainty is notably larger for low SZAs, with values for 32° doubling the values computed for 65° for wavelengths longer than 320 nm. In fact, the SZA is the most influential factor in determining the range of uncertainty values.

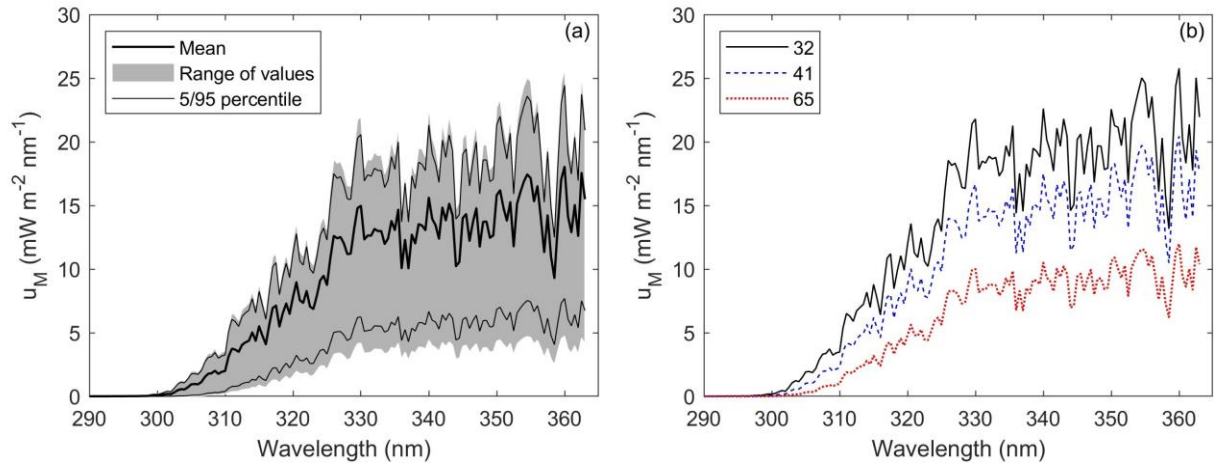

Figure 6: Combined standard uncertainty of Brewer #150 UV irradiance spectra. (a) Mean, range of values and 5th and 95th percentiles of the UV irradiance combined standard uncertainty during the study period (from 10 September to 20 October 21). (b) Combined standard uncertainty of the UV irradiance measured on 10 September 2021 at three zenith angles: 32°, 41°, and 65°.

To illustrate the order of magnitude of the combined standard uncertainty compared to the solar irradiance spectra, an example scan is presented in Fig. 7 alongside its uncertainty (±1σ). Both linear and logarithmic scales are used to clarify the uncertainty contribution at short and large wavelengths.

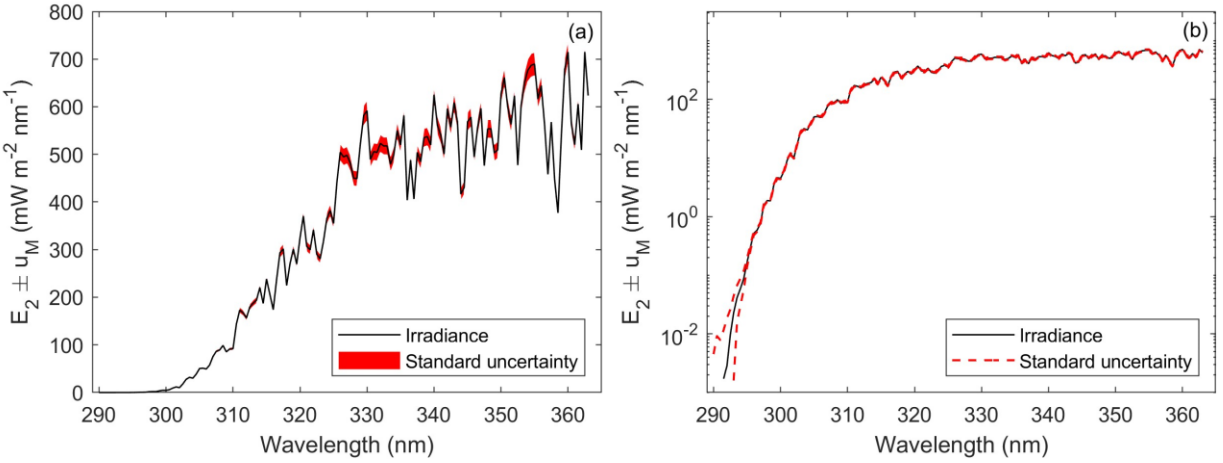

Figure 7: Solar irradiance and its combined standard uncertainty (±1σ) for a spectrum measured on 10 September 2021 at a SZA of 32 °C in (a) linear scale and (b) logarithmic scale.

Fig. 7a shows that the absolute combined standard uncertainty is relatively small compared to the actual solar spectrum (around 4 % for wavelengths above 310 nm). Due to the abrupt increase of

solar irradiance with wavelength (4 orders of magnitude), it may seem that the uncertainty is negligible at short wavelengths. However, if the same spectrum is represented in logarithmic scale (Fig. 7b) it becomes visible that the combined standard uncertainty is large, exceeding 100 % for wavelengths below 295 nm.

In addition to the absolute values of the combined standard uncertainty, the analysis of its relative values is of great interest due to the large variation of UV irradiance with wavelength. Thus, Fig. 8 illustrates the relative values of the UV irradiance combined standard uncertainty, $\boldsymbol{u}_M$ / $\boldsymbol{E}_2$, with respect to the wavelength. For wavelengths below 300 nm, the average relative uncertainties exceed 100 %. This mean value was expected since the irradiance comes close to zero as wavelength approaches 290 nm. For wavelengths above 300 nm, the mean relative combined standard uncertainty slowly decreases from 5.1 % at 300 nm to 3.5 % at 363 nm. Furthermore, some spikes can be observed at specific wavelengths such as 302, 304.5 or 306.5 nm (Fig. 8a). They are caused by wavelength misalignment and have been already reported in other Monte Carlo simulations (Cordero et al., 2008a; Schinke et al., 2020). Although they result in high uncertainties at the mentioned specific wavelengths, their effect on the average uncertainty is limited.

Regarding the variability, the 290–300 nm region shows the largest variability, of about 300 %. This extreme high value is mainly produced by wavelength shift as well as PMT and thermal noise. These uncertainty sources have a greater effect for very low signals, which are recorded at short wavelengths and large SZAs. Their effect could be reduced by checking the wavelength alignment weekly or expanding the scan duration in an effort to decrease noise and instabilities. On the other hand, between 310 and 363 nm the uncertainty is independent of the SZA and as a result the variability, defined as the difference between the 5th and the 95th percentiles, levels off at around 1.3 %. This angular dependency agrees with the values reported by Bernhard and Seckmeyer (1999).

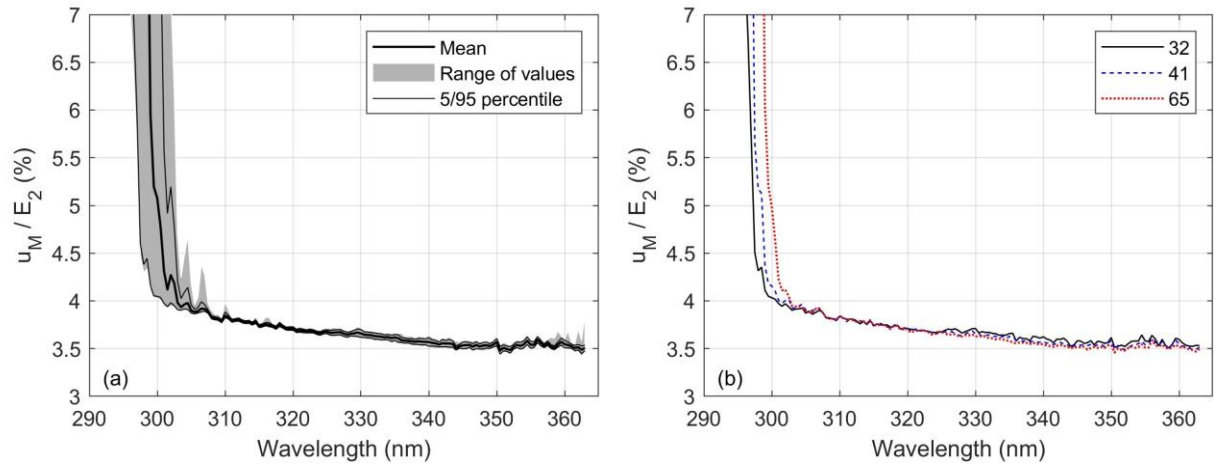

Figure 8: Relative combined standard uncertainty of the Brewer #150 UV irradiance spectra. (a) Range of values, mean and 5th and 95th percentiles of the relative combined standard uncertainty during the study period. (b) Relative combined standard uncertainty of the UV irradiance measured on 10 September 2021 at three solar zenith angles: 32°, 41°, and 65°.

Furthermore, the main influences in the combined standard uncertainty can be studied by separating the contribution from the uncertainties committed during the calibration and the ones affecting the outdoors measurements (these uncertainty sources are shown in Fig. 3). In this way, the dominant sources become visible.

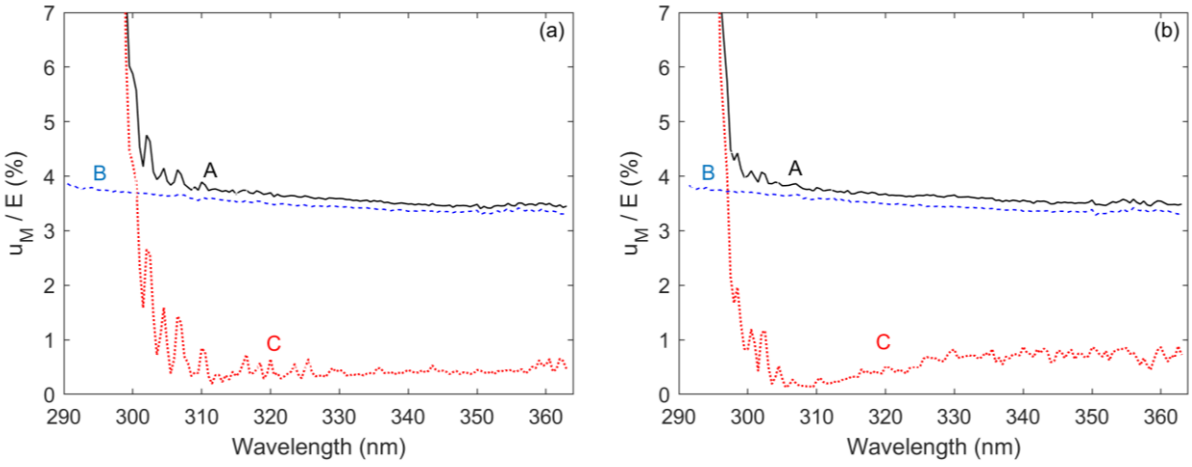

Figure 9: Contributions to the combined relative uncertainty of Brewer #150 UV irradiance measured on 10 September at a solar angle of (a) 65° and (b) 32°. Curve A depicts the combined relative uncertainty. Curve B and C show the contributions to the overall uncertainty depicted in curve A. The uncertainties in curve B were obtained considering only the uncertainty sources

affecting the radiometric calibration. The uncertainties in curve C were calculated considering the uncertainty sources of the outdoors measurements.

Figure 9 shows the results of such calculation. The influence of the radiometric calibration is important for wavelengths larger than 305 nm. For this wavelength range (305 – 363 nm), the mean relative uncertainty (curve A) is 3.6 % while the uncertainties arising from the radiometric calibration (curve B) and the outdoors measurements (curve C) are 3.4 % and 0.5 % respectively. The uncertainty source responsible for this effect is the stability of Brewer #150, ranging from 3.8 % at 290 nm to 3.2 % at 363 nm. Since the uncertainties arising from the calibration have no dependence on SZA, the relative combined standard uncertainty shows no significant angular dependence in this wavelength range. On the other hand, for wavelengths below 300 nm, the uncertainties arising from the measurements outdoors have the largest impact. This effect is due to PMT noise, dark counts, and wavelength misalignment. Furthermore, since the uncertainties from the outdoors measurements have a considerable angular dependence, the relative combined standard uncertainty shows the same dependence.

The spectral expanded uncertainty $\boldsymbol{U}_{\mathrm{M}}$ can be obtained from the combined standard uncertainty multiplied by a coverage factor of $k = 2$. Therefore, the mean relative expanded uncertainty of Brewer #150 irradiance measurements varies between 10 % at 300 nm and 7 % at 363 nm. Since the histogram of the spectral irradiance, as shown in Fig. 10, is nearly a Gaussian distribution, the irradiance should lie in this interval with a probability of approximately 95%. The normality of the data was visually confirmed through a quantile-quantile (QQ) plot.

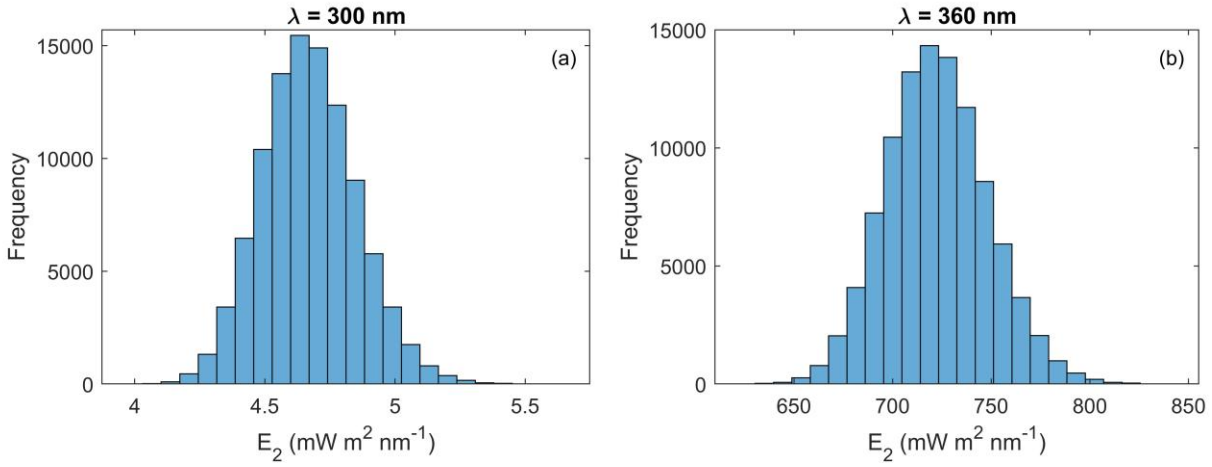

Figure 10: Histogram of the simulated irradiance at a solar zenith angle of 32° resulting from 10^5 iterations. (a) Global UV irradiance at 300 nm and (b) Global UV irradiance at 360 nm. The

632 expected values and standard deviations are (a) 4.67 mW m^{-2} nm^{-1} and 0.18 mW m^{-2} nm^{-1}; (b)
633 722.50 mW m^{-2} nm^{-1} and 25.69 mW m^{-2} nm^{-1}.

634 Finally, the relative combined standard uncertainty of Brewer #150 can be compared with the
635 one obtained in previous studies. Garane et al. (2006) used a MKIII Brewer and conducted an
636 uncertainty analysis by applying the law of propagation of uncertainties (LPU). Their study
637 reports a 1σ uncertainty of approximately 5 % for the 290–363 nm range. This value is similar to
638 the one obtained in our work at 300 nm. Furthermore, the shape of the spectral and angular
639 dependency of Brewer #150 irradiance combined standard uncertainty is similar to the ones
640 described in other publications (Bernhard & Seckmeyer, 1999; Gröbner et al., 2005). On the
641 other hand, the expanded uncertainty of Brewer #150 can also be compared to the values
642 reported in other studies for double monochromator spectroradiometers. Fountoulakis et al.
643 (2020) used a Bentham DTM300 double monochromator and reported an expanded uncertainty
644 at 300 nm of the order of 10–12 % for SZAs lower than 75°. Gröbner et al. (2005) conducted an
645 uncertainty analysis for the QASUME and found an expanded uncertainty of 6.2 % for the 310–
646 400 nm range and SZAs lower than 50°. Therefore, Brewer #150 average expanded and relative
647 combined standard uncertainty is comparable to those of other commercial double
648 monochromators.

649 **5 Conclusions**

650 The combined standard uncertainty of Brewer #150 global UV spectra was obtained using a
651 Monte Carlo uncertainty evaluation. The spectral measurements used were recorded from 10
652 September to 20 October 2021, after an absolute calibration was performed during the XVI
653 Intercomparison Campaign of the RBCC-E. Only cloud-free conditions have been considered,
654 resulting in 599 UV scans.

655 For the uncertainty evaluation, Brewer #150 was thoroughly characterised and its uncertainty
656 sources studied in detail. In the Monte Carlo simulation, the effect of these uncertainty sources
657 was considered by calculating the irradiance a large number of times ($N = 10^5$) while varying the
658 uncertainty sources according to their assigned PDF.

659 Brewer #150 irradiance combined standard uncertainty depends significantly on wavelength and
660 SZA, increasing as wavelength rises and SZA declines. Regarding the relative combined

standard uncertainty, it also shows a considerable spectral dependency. For the 310–363 nm region, it is mostly of the order of 3–4 %. In this wavelength range, the uncertainty is independent of solar zenith angle. In fact, the variability due to SZA is of the order of ~1 %. The reason is that at this wavelength region the uncertainties arising from the radiometric calibration, in particular the stability, have the biggest impact. Since these uncertainty sources have no significant angular dependence, the relative uncertainty also shows no SZA dependency. However, for wavelengths below 310 nm, the relative combined standard uncertainty does depend significantly on SZA, decreasing as SZA increases. This is produced by three uncertainty sources whose effects affect mainly short wavelengths: PMT noise, dark counts, and wavelength shift.

The expanded uncertainty varies from 10 % at 300 nm to 7 % at 363 nm. Consequently, the UV dataset of Brewer #150 is suitable for model and satellite validation as well as climatological studies. However, the determination of UV trends due to ozone change may be limited, as Brewer #150 combined standard uncertainty is higher than the change of erythemal irradiance produced by a 1 % change in ozone. Thus, work is needed to further reduce the uncertainty in order to accurately detect such trends. For Brewer #150, this could be achieved by improving its temporal stability.

Although a Brewer spectrophotometer was used in this work, the methodology employed to evaluate its uncertainty can be applied to other double monochromator instruments. Furthermore, it could be adapted for CCD-array spectroradiometers if their stray light is properly characterised and included in the uncertainty evaluation.

Acknowledgments

The authors declare that they have no conflict of interest. This research has been supported by the National Institute of Aerospace Technology (project no. S.OJE04001). It is also part of the Grant TED2021-130532A-I00 funded by MCIN/AEI/10.13039/501100011033 and by the "European Union NextGenerationEU/PRTR".

We also thank Victoria E. Cachorro Revilla and Margarita Yela González for their effort in establishing and maintaining AERONET El Arenosillo/Huelva site.

Open Research

The ozone data used for the Brewer cosine correction in the study are available at https://eubrewnet.aemet.es/eubrewnet; The software SHICrivm used for the obtention of wavelength shift is available at https://www.rivm.nl/en/uv-ozone-layer-and-climate/shicrivm/download; The aerosol data used for the Brewer cosine correction are available at https://aeronet.gsfc.nasa.gov/cgi-bin/data_display_aod_v3?site=El_Arenosillo&nachal=2&level=1; The dataset used for the uncertainty evaluation is available at Zenodo via https://doi.org/10.5281/zenodo.8046474. The software used for the implementation of the Monte Carlo technique is available at Zenodo via https://doi.org/10.5281/zenodo.8046562 with license Creative Commons Attribution 4.0 International; The figures in this manuscript are prepared using MATLAB software (URL: https://es.mathworks.com/products/matlab.html).

References

Andrady, A. L., Heikkilä, A. M., Pandey, K. K., Bruckman, L. S., White, C. C., Zhu, M., & Zhu, L. (2023). Effects of UV radiation on natural and synthetic materials. *Photochemical and Photobiological Sciences*, *22*(5), 1177–1202. https://doi.org/10.1007/s43630-023-00377-6

Antón, M., Cachorro, V. E., Vilaplana, J. M., Toledano, C., Krotkov, N. A., Arola, A., & de La Morena, B. (2010). Comparison of UV irradiances from Aura/Ozone Monitoring Instrument (OMI) with Brewer measurements at El Arenosillo (Spain) – Part 1: Analysis of parameter influence. *Atmospheric Chemistry and Physics*, *10*(13), 5979–5989. https://doi.org/10.5194/acp-10-5979-2010

Antón, M., Serrano, A., Cancillo, M. L., & Vilaplana, J. M. (2011). Quality assurance of broadband erythemal radiometers at the Extremadura UV Monitoring Network (Southwestern Spain). *Atmospheric Research*, *100*(1), 83–92. https://doi.org/10.1016/j.atmosres.2010.12.029

Arola, A., Lakkala, K., Bais, A., Kaurola, J., Meleti, C., & Taalas, P. (2003). Factors affecting short- and long-term changes of spectral UV irradiance at two European stations. *Journal of Geophysical Research: Atmospheres*, *108*(17). https://doi.org/10.1029/2003jd003447

Bais, A. F., Gardiner, B. G., Slaper, H., Blumthaler, M., Bernhard, G., McKenzie, R., Webb, A. R., Seckmeyer, G., Kjeldstad, B., Koskela, T., Kirsch, P. J., Gröbner, J., Kerr, J. B., Kazadzis, S., Leszcynski, K., Wardle, D., Josefsson, W., Brogniez, C., Gillotay, D., Reinen, H., Weihs, P., Svenoe, T., Eriksen, P., Kuik, F., & Redondas, A. (2001). SUSPEN intercomparison of ultraviolet spectroradiometers. *Journal of Geophysical Research: Atmospheres*, *106*(D12), 12509–12525. https://doi.org/10.1029/2000JD900561

Bais, A. F., Kazadzis, S., Balis, D., Zerefos, C. S., & Blumthaler, M. (1998). Correcting global solar ultraviolet spectra recorded by a Brewer spectroradiometer for its angular response error. *Applied Optics*, *37*(27), 6339. https://doi.org/10.1364/AO.37.006339

Bais, A. F., Lucas, R. M., Bornman, J. F., Williamson, C. E., Sulzberger, B., Austin, A. T., Wilson, S. R., Andrady, A. L., Bernhard, G., McKenzie, R. L., Aucamp, P. J., Madronich, S., Neale, R. E., Yazar, S., Young, A. R., de Gruijl, F. R., Norval, M., Takizawa, Y., Barnes, P. W., … Heikkilä, A. M. (2018). Environmental effects of ozone depletion, UV radiation and interactions with climate change: UNEP Environmental Effects Assessment Panel, update 2017. *Photochemical & Photobiological Sciences*, *17*(2), 127–179. https://doi.org/10.1039/c7pp90043k

Bais, A. F., Zerefos, C. S., & McElroy, C. T. (1996). Solar UVB measurements with the double- and single-monochromator Brewer ozone spectrophotometers. *Geophysical Research Letters*, *23*(8), 833–836. https://doi.org/10.1029/96GL00842

Barnes, P. W., Robson, T. M., Zepp, R. G., Bornman, J. F., Jansen, M. A. K., Ossola, R., Wang, Q. W., Robinson, S. A., Foereid, B., Klekociuk, A. R., Martinez-Abaigar, J., Hou, W. C., Mackenzie, R., & Paul, N. D. (2023). Interactive effects of changes in UV radiation and climate on terrestrial ecosystems,

biogeochemical cycles, and feedbacks to the climate system. *Photochemical & Photobiological Sciences*, *22*(5), 1049–1091. https://doi.org/10.1007/s43630-023-00376-7

Bernhard, G. (2011). Trends of solar ultraviolet irradiance at Barrow, Alaska, and the effect of measurement uncertainties on trend detection. *Atmospheric Chemistry and Physics*, *11*(24), 13029–13045. https://doi.org/10.5194/acp-11-13029-2011

Bernhard, G., & Seckmeyer, G. (1999). Uncertainty of measurements of spectral solar UV irradiance. *Journal of Geophysical Research Atmospheres*, *104*(D12), 14321–14345. https://doi.org/10.1029/1999JD900180

Bernhard, G., Booth, C. R., Ehramjian, J. C., Stone, R., & Dutton, E. G. (2007). Ultraviolet and visible radiation at Barrow, Alaska: Climatology and influencing factors on the basis of version 2 National Science Foundation network data. *Journal of Geophysical Research Atmospheres*, *112*(9), D09101. https://doi.org/10.1029/2006JD007865

BIPM, IEC, IFCC, ILAC, ISO, IUPAC, & OIML. (2008). Evaluation of Measurement Data – Supplement 1 to the Guide to the Expression of Uncertainty in Measurement – Propagation of distributions using a Monte Carlo method. Bureau International des Poids et Mesures, JCGM 101

Cachorro, V. E., Toledano, C., Antón, M., Berjón, A., de Frutos, A., Vilaplana, J. M., Arola, A., & Krotkov, N. A. (2010). Comparison of UV irradiances from Aura/Ozone Monitoring Instrument (OMI) with Brewer measurements at El Arenosillo (Spain) – Part 2: Analysis of site aerosol influence. *Atmospheric Chemistry and Physics*, *10*(23), 11867–11880. https://doi.org/10.5194/acp-10-11867-2010

Cachorro, V. E., Vergaz, R., Martin, M. J., de Frutos, A. M., Vilaplana, J. M., & de la Morena, B. (2002). Measurements and estimation of the columnar optical depth of tropospheric aerosols in the UV spectral region. *Annales Geophysicae*, *20*(4), 565–574. https://doi.org/10.5194/angeo-20-565-2002

Cancillo, M. L., Serrano, A., Anton, M., Garcia, J. A., Vilaplana, J., & de la Morena, B. (2005). An Improved Outdoor Calibration Procedure for Broadband Ultraviolet Radiometers. *Photochemistry and Photobiology*, *81*(4), 860–865. https://doi.org/10.1562/2005-01-12-RA-412

Cappellani, F., & Kochler, C. (2000). Temperature effects correction in a Brewer MKIV spectrophotometer for solar UV measurements. *Journal of Geophysical Research: Atmospheres*, *105*(D4), 4829–4831. https://doi.org/10.1029/1999JD900254

Cordero, R. R., Seckmeyer, G., & Labbe, F. (2008a). Cosine error influence on ground-based spectral UV irradiance measurements. *Metrologia*, *45*(4), 406–414. https://doi.org/10.1088/0026-1394/45/4/005

Cordero, R. R., Seckmeyer, G., Pissulla, D., Dasilva, L., & Labbe, F. (2008b). Uncertainty evaluation of spectral UV irradiance measurements. *Measurement Science and Technology*, *19*(4). https://doi.org/10.1088/0957-0233/19/4/045104

Cordero, R. R., Seckmeyer, G., Riechelmann, S., Damiani, A., & Labbe, F. (2012). Monte carlo-based uncertainty analysis of UV array spectroradiometers. *Metrologia*, *49*(6), 745–755. https://doi.org/10.1088/0026-1394/49/6/745

De Bock, V., De Backer, H., Van Malderen, R., Mangold, A., & Delcloo, A. (2014). Relations between erythemal UV dose, global solar radiation, total ozone column and aerosol optical depth at Uccle, Belgium. *Atmospheric Chemistry and Physics*, *14*(22), 12251–12270. https://doi.org/10.5194/acp-14-12251-2014

Diémoz, H., Siani, A. M., Redondas, A., Savastiouk, V., Mcelroy, C. T., Navarro-Comas, M., & Hase, F. (2014). Improved retrieval of nitrogen dioxide (NO2) column densities by means of MKIV Brewer spectrophotometers. *Atmospheric Measurement Techniques*, *7*(11), 4009–4022. https://doi.org/10.5194/amt-7-4009-2014

D'Orazio, J., Jarrett, S., Amaro-Ortiz, A., & Scott, T. (2013). UV radiation and the skin. *International Journal of Molecular Sciences*, *14*(6), 12222–12248. https://doi.org/10.3390/ijms140612222

Farman, J. C., Gardiner, B. G., & Shanklin, J. D. (1985). Large losses of total ozone in Antarctica reveal seasonal ClOx/NOx interaction. *Nature*, *315*(6016), 207–210. https://doi.org/10.1038/315207a0

Fioletov, V. E., Kerr, J. B., McArthur, L. J. B., Wardle, D. I., & Mathews, T. W. (2003). Estimating UV Index Climatology over Canada. *Journal of Applied Meteorology*, *42*(3), 417–433. https://doi.org/10.1175/1520-0450(2003)042<0417:EUICOC>2.0.CO;2

Fioletov, V. E., McArthur, L. J. B., Kerr, J. B., & Wardle, D. I. (2001). Long-term variations of UV-B irradiance over Canada estimated from Brewer observations and derived from ozone and pyranometer measurements. *Journal of Geophysical Research: Atmospheres*, *106*(D19), 23009–23027. https://doi.org/10.1029/2001JD000367

Fountoulakis, I., Bais, A. F., Fragkos, K., Meleti, C., Tourpali, K., & Zempila, M. M. (2016a). Short- and long-term variability of spectral solar UV irradiance at Thessaloniki, Greece: Effects of changes in aerosols, total ozone and clouds. *Atmospheric Chemistry and Physics*, *16*(4), 2493–2505. https://doi.org/10.5194/acp-16-2493-2016

Fountoulakis, I., Diémoz, H., Siani, A. M., Hülsen, G., & Gröbner, J. (2020). Monitoring of solar spectral ultraviolet irradiance in Aosta, Italy. *Earth System Science Data*, *12*(4), 2787–2810. https://doi.org/10.5194/essd-12-2787-2020

Fountoulakis, I., Redondas, A., Bais, A. F., Rodriguez-Franco, J. J., Fragkos, K., & Cede, A. (2016b). Dead time effect on the Brewer measurements: correction and estimated uncertainties. *Atmospheric Measurement Techniques*, *9*(4), 1799–1816. https://doi.org/10.5194/amt-9-1799-2016

Fountoulakis, I., Redondas, A., Lakkala, K., Berjon, A., Bais, A. F., Doppler, L., Feister, U., Heikkila, A., Karppinen, T., Karhu, J. M., Koskela, T., Garane, K., Fragkos, K., & Savastiouk, V. (2017). Temperature

dependence of the Brewer global UV measurements. *Atmospheric Measurement Techniques*, *10*(11), 4491–4505. https://doi.org/10.5194/amt-10-4491-2017

Garane, K., Bais, A. F., Kazadzis, S., Kazantzidis, A., & Meleti, C. (2006). Monitoring of UV spectral irradiance at Thessaloniki (1990–2005): Data re-evaluation and quality control. *Annales Geophysicae*, *24*(12), 3215–3228. https://doi.org/10.5194/angeo-24-3215-2006

García-Corral, L. S., Duarte, C. M., & Agusti, S. (2020). Impact of UV radiation on plankton net community production: Responses in Western Australian estuarine and coastal waters. *Marine Ecology Progress Series*, *651, 45*–56. https://doi.org/10.3354/meps13456

Glandorf, M., Arola, A., Bais, A., & Seckmeyer, G. (2005). Possibilities to detect trends in spectral UV irradiance. *Theoretical and Applied Climatology*, *81*(1–2), 33–44. https://doi.org/10.1007/s00704-004-0109-9

Gónzalez, C., Vilaplana, J. M., & Serrano, A. (2023). Brewer #150 UV measurements and ancillary data needed for its uncertainty evaluation (Version 1). [Dataset]. Zenodo. https://doi.org/10.5281/zenodo.8046474

González, C., Vilaplana, J. M. & Serrano, A. (2023, June 19). Monte Carlo simulation for the uncertainty evaluation of Brewer UV spectra (Version 1.0) [Software]. Zenodo. https://doi.org/10.5281/zenodo.8046562

Gröbner, J. (2003). Improved entrance optic for global irradiance measurements with a Brewer spectrophotometer. *Applied Optics*, *42*(18), 3516–3521. https://doi.org/10.1364/AO.42.003516

Gröbner, J., & Blumthaler, M. (2007). Experimental determination of the reference plane of shaped diffusers by solar ultraviolet measurements. *Optics Letters*, *32*(1), 80–82. https://doi.org/10.1364/OL.32.000080

Gröbner, J., Schreder, J., Kazadzis, S., Bais, A. F., Blumthaler, M., Görts, P., Tax. R., Koskela, T., Seckmeyer, G., Webb, A. R., & Rembges, D. (2005). Traveling reference spectroradiometer for routine quality assurance of spectral solar ultraviolet irradiance measurements. *Applied Optics*, *44*(25), 5321–5331. https://doi.org/10.1364/AO.44.005321

Gröbner, J., Wardle, D. I., McElroy, C. T., & Kerr, J. B. (1998). Investigation of the wavelength accuracy of Brewer spectrophotometers. *Applied Optics*, *37*(36), 8352–8360. https://doi.org/10.1364/AO.37.008352

Harris, N. R. P., Ancellet, G., Bishop, L., Hofmann, D. J., Kerr, J. B., McPeters, R. D., Prendez, M., Randel, W. J., Staehelin, J., Subbraya, B. H., Volz-Thomas, A., Zawodny J., & Zerefos, C. S. (1997). Trends in stratospheric and free tropospheric ozone. *Journal of Geophysical Research: Atmospheres*, *102*(D1), 1571–1590. https://doi.org/10.1029/96JD02440

Hart, P. H., & Norval, M. (2018). Ultraviolet radiation-induced immunosuppression and its relevance for skin carcinogenesis. *Photochemical and Photobiological Sciences*, *17*(12), 1872–1884. https://doi.org/10.1039/c7pp00312a

Hovila, J., Mustonen, M., Kärhä, P., & Ikonen, E. (2005). Determination of the diffuser reference plane for accurate illuminance responsivity calibrations. *Applied Optics*, *44*(28), 5894–5898. https://doi.org/10.1364/AO.44.005894

Hülsen, G., Gröbner, J., Nevas, S., Sperfeld, P., Egli, L., Porrovecchio, G., & Smid, M. (2016). Traceability of solar UV measurements using the Qasume reference spectroradiometer. *Applied Optics*, *55*(26), 7265–7275. https://doi.org/10.1364/AO.55.007265

Kärhä, P., Vaskuri, A., Mäntynen, H., Mikkonen, N., & Ikonen, E. (2017). Method for estimating effects of unknown correlations in spectral irradiance data on uncertainties of spectrally integrated colorimetric quantities. *Metrologia*, *54*(4), 524–534. https://doi.org/10.1088/1681-7575/aa7b39

Kerr, J. B. (2002). New methodology for deriving total ozone and other atmospheric variables from Brewer spectrophotometer direct sun spectra. *Journal of Geophysical Research: Atmospheres*, *107*(D23), 4731. https://doi.org/10.1029/2001JD001227

Kerr, J. B., & McElroy, C. T. (1993). Evidence for Large Upward Trends of Ultraviolet-B Radiation Linked to Ozone Depletion. *Science*, *262*(5136), 1032–1034. https://doi.org/10.1126/science.262.5136.1032

Kimlin, M. G. (2004). The climatology of Vitamin D producing ultraviolet radiation over the United States. *The Journal of Steroid Biochemistry and Molecular Biology*, *89–90*, 479–483. https://doi.org/10.1016/j.jsbmb.2004.03.111

Lakkala, K., Arola, A., Heikkilä, A., Kaurola, J., Koskela, T., Kyrö, E., Lindfors, A., Meinander, O., Tanskanen, A., Gröbner, J., & Hülsen, G. (2008). Quality assurance of the Brewer spectral UV measurements in Finland. *Atmospheric Chemistry and Physics*, *8*(13), 3369–3383. https://doi.org/10.5194/acp-8-3369-2008

Lakkala, Kaisa, Heikkilä, A., Kärhä, P., Ialongo, I., Karppinen, T., Karhu, J. M., Lindfors, A. V., & Meinander, O. (2017). 25 years of spectral UV measurements at Sodankylä. *AIP Conference Proceedings*, *1810*, 110006. https://doi.org/10.1063/1.4975568

Lumi, X., Dučić, T., Kreuzer, M., Hawlina, M., & Andjelic, S. (2021). UV Effect on Human Anterior Lens Capsule Macro-Molecular Composition Studied by Synchrotron-based FTIR Micro-Spectroscopy. *International Journal of Molecular Sciences*, *22*(10), 5249–5261. https://doi.org/10.3390/ijms22105249

Manninen, P., Hovila, J., Seppälä, L., Kärhä, P., Ylianttila, L., & Ikonen, E. (2006). Determination of distance offsets of diffusers for accurate radiometric measurements. *Metrologia*, *43*(2), S120–S124. https://doi.org/10.1088/0026-1394/43/2/S24

Mayer, B., Seckmeyer, G., & Kylling, A. (1997). Systematic long-term comparison of spectral UV measurements and UVSPEC modeling results. *Journal of Geophysical Research Atmospheres*, *102*(7), 8755–8767. https://doi.org/10.1029/97jd00240

McKenzie, R., Connor, B., & Bodeker, G. (1999). Increased Summertime UV Radiation in New Zealand in Response to Ozone Loss. *Science*, *285*(5434), 1709–1711. https://doi.org/10.1126/science.285.5434.1709

Meinander, O., Josefsson, W., Kaurola, J., Koskela, T., & Lakkala, K. (2003). Spike detection and correction in Brewer spectroradiometer ultraviolet spectra. *Optical Engineering*, *42*(6), 1812–1819.

Morgenstern, O., Braesicke, P., Hurwitz, M. M., O'Connor, F. M., Bushell, A. C., Johnson, C. E., & Pyle, J. A. (2008). The World Avoided by the Montreal Protocol. *Geophysical Research Letters*, *35*(16), L16811. https://doi.org/10.1029/2008GL034590

Neale, P. J., Williamson, C. E., Banaszak, A. T., Häder, D. P., Hylander, S., Ossola, R., Rose, K. C., Wängberg, S. Å., & Zepp, R. (2023). The response of aquatic ecosystems to the interactive effects of stratospheric ozone depletion, UV radiation, and climate change. *Photochemical & Photobiological Sciences*, *22*(5), 1093–1127. https://doi.org/10.1007/s43630-023-00370-z

Newman, P. A., Oman, L. D., Douglass, A. R., Fleming, E. L., Frith, S. M., Hurwitz, M. M., Kawa, S. R., Jackman, C. H., Krotkov, N. A., Nash, E. R., Nielsen, J. E., Pawon, S., Stolarski, R. S., & Velders, G. J. M. (2009). What would have happened to the ozone layer if chlorofluorocarbons (CFCs) had not been regulated? *Atmospheric Chemistry and Physics*, *9*(6), 2113–2128. https://doi.org/10.5194/acp-9-2113-2009

Prather, M., Midgley, P., Rowland, F. S., & Stolarski, R. (1996). The ozone layer: the road not taken. *Nature*, *381*(6583), 551–554. https://doi.org/10.1038/381551a0

Redondas, A., Berjón, A., López-Solano, J., Carreño, V., León-Luis, S. F., & Santana, D. (2020). "El Arenosillo" 2019 Campaign Report (GAW Report No. 257). Joint publication of State Meteorological Agency (AEMET) and Wolrd Meteorological Organization (WMO)

Schafer, J. S., Saxena, V. K., Wenny, B. N., Barnard, W., & De Luisi, J. J. (1996). Observed influence of clouds on ultraviolet-B radiation. *Geophysical Research Letters*, *23*(19), 2625–2628. https://doi.org/10.1029/96GL01984

Schinke, C., Pollex, H., Hinken, D., Wolf, M., Bothe, K., Kröger, I., Nevas, S., & Winter, S. (2020). Calibrating spectrometers for measurements of the spectral irradiance caused by solar radiation. *Metrologia*, *57*(6), 065027. https://doi.org/10.1088/1681-7575/abafc5

Schmähling, F., Wübbeler, G., Krüger, U., Ruggaber, B., Schmidt, F., Taubert, R. D., Sperling, A., & Elster, C. (2018). Uncertainty evaluation and propagation for spectral measurements. *Color Research & Application*, *43*(1), 6–16. https://doi.org/10.1002/col.22185

Seckmeyer, G., Bais, A., Bernhard, G., Blumthaler, M., Booth, C., Disterhoft, P., Eriksen, P., McKenzie, R., Miyauchi, M., & Roy, C. (2001). Instruments to measure solar ultraviolet irradiance. Part 1: Spectral instruments (GAW Report No. 125). World Meteorological Organization (WMO)

Seckmeyer, G., Mayer, B., Erb, R., & Bernhard, G. (1994). UV-B in Germany higher in 1993 than in 1992. *Geophysical Research Letters*, *21*(7), 577–580. https://doi.org/10.1029/94GL00567

Seckmeyer, G., Pissulla, D., Glandorf, M., Henriques, D., Johnsen, B., Webb, A., Siani, A. M., Bais, A., Kjeldstad, B., Brogniez, C., Lenoble, J., Gardiner, B., Kirsch, P., Koskela, T., Kaurola, J., Uhlmann, B., Slaper, H., den Outer, P., Janouch, M., Werle, P., Gröbner, J., Mayer, B., de la Casiniere, A., Smic, S., & Carvalho, F. (2008). Variability of UV Irradiance in Europe. *Photochemistry and Photobiology*, *84*(1), 172–179. https://doi.org/10.1111/j.1751-1097.2007.00216.x

Slaper, H., Reinen, H. A. J. M., Blumthaler, M., Huber, M., & Kuik, F. (1995). Comparing ground-level spectrally resolved solar UV measurements using various instruments: A technique resolving effects of wavelength shift and slit width. *Geophysical Research Letters*, *22*(20), 2721–2724. https://doi.org/10.1029/95GL02824

Vaskuri, A., Kärhä, P., Egli, L., Gröbner, J., & Ikonen, E. (2018). Uncertainty analysis of total ozone derived from direct solar irradiance spectra in the presence of unknown spectral deviations. *Atmospheric Measurement Techniques*, *11*(6), 3595–3610. https://doi.org/10.5194/amt-11-3595-2018

Wachter, I., Štefko, T., Rantuch, P., Martinka, J., & Pastierová, A. (2021). Effect of UV Radiation on Optical Properties and Hardness of Transparent Wood. *Polymers*, *13*(13), 2067–2080. https://doi.org/10.3390/polym13132067

Weatherhead, E. C., Reinsel, G. C., Tiao, G. C., Meng, X. L., Choi, D., Cheang, W. K., Keller, T., DeLuisi, J., Wuebbles, D. J., Kerr, J. B., Miller, A. J., Oltmans, S. J., & Frederick, J. E. (1998). Factors affecting the detection of trends: Statistical considerations and applications to environmental data. *Journal of Geophysical Research Atmospheres*, *103*(D14), 17149–17161. https://doi.org/10.1029/98JD00995

Weatherhead, E., Theisen, D., Stevermer, A., Enagonio, J., Rabinovitch, B., Disterhoft, P., Lantz, K., Meltzer, R., Sabburg, J., DeLuisi, J., Rives, J., & Shreffler, J. (2001). Temperature dependence of the Brewer ultraviolet data. *Journal of Geophysical Research: Atmospheres*, *106*(D24), 34121–34129. https://doi.org/10.1029/2001JD000625

Webb, A. R., Gardiner, B. G., Blumthaler, M., Forster, P., Huber, M., & Kirsch, P. J. (1994). A laboratory investigation of two ultraviolet spectroradiometers. *Photochemistry and Photobiology*, *60*(1), 84–90. https://doi.org/10.1111/j.1751-1097.1994.tb03947.x

Webb, A. R., Gardiner, B. G., Martin, T. J., Leszcynski, K., Metzdorf, J., & Mohnen, V. A. (1998). Guidelines for Site Quality Control of UV Monitoring (GAW Report No. 126). World Meteorological Organization (WMO)

Ylianttila, L., & Schreder, J. (2005). Temperature effects of PTFE diffusers. *Optical Materials*, *27*(12), 1811–1814. https://doi.org/10.1016/j.optmat.2004.11.008

Zerefos, C. S., Balis, D. S., Bais, A. F., Gillotay, D., Simon, P. C., Mayer, B., & Seckmeyer, G. (1997). Variability of UV-B at four stations in Europe. *Geophysical Research Letters*, *24*(11), 1363–1366. https://doi.org/10.1029/97GL01177

Zerefos, C. S., Tourpali, K., Eleftheratos, K., Kazadzis, S., Meleti, C., Feister, U., Koskela, T., & Heikkilä, A. (2012). Evidence of a possible turning point in solar UV-B over Canada, Europe and Japan. *Atmospheric Chemistry and Physics*, *12*(5), 2469–2477. https://doi.org/10.5194/acp-12-2469-2012